COMPUTATION OF UNSTEADY TRANSONIC WING PRESSURES BY A 2D-3D CORRECTION AND INVERSE METHODS

by
K. Dau, M.A.Sc.
Messerschmitt-Bölkow-Blohm GmbH
Bremen, Germany

Abstract

A method is presented for calculating unsteady transonic aerodynamic forces on wings of moderate to large aspect ratio. The wing is represented by equivalent profiles derived from measured pressures and an inverse subsonic method. Pressures are calculated on these profiles by a standard 2-D TSP code, and subsequently corrected for 3-D flow by means of a correction matrix based on Doublet-lattice theory. The equations for the correction matrix are derived. The calculated unsteady results are compared with measured pressures.

I. Introduction

Standard methods for calculating unsteady aerodynamic pressures in subsonic flow such as the Doublet-Lattice (DL) method fail when applied to wings with well-developed shocks. On the other hand, more elaborate 3-D codes based on Finite Difference (FD) or Finite Element (FE) methods are at present rather expensive to use in routine work such as flutter validation procedures. To bridge the gap this paper presents a method for calculating steady pressures on a wing of moderate to large aspect ratio in transonic flow by making maximum use of existing computing codes and experimental data.

The wing is represented by equivalent profiles derived by means of an inverse subsonic method due to Weber (1) using measured steady pressure data. The procedure is described in Sect II. A standard 2-D transonic TSP code (2) is used to calculate the pressures on the equivalent profiles. The pressures are then corrected for 3-D effects by means of a correction matrix, which is derived in Sect. III. The calculated 3-D pressures are compared with measured unsteady pressures.

Similar methods were developed independently at NLR (3,4), where the corrections were made to section coefficients rather than pressures.

II. Computation of equivalent profiles

Steady transonic pressure distributions Cp calculated by potential methods generally show a mismatch with measured pressures, especially in the position and size of the shock, mainly because of boundary layer effects, and sometimes because of small uncertainties in the measured free-steam Mach number and incidence. It is well known that if the calculated unsteady pressures are to show any semblance to the measured ones, the calculated steady pressures must agree with the corresponding measured steady pressure distribution. This is sometimes achieved in calculations by raising the trailing edge, varying the Mach number, etc. To eliminate the mismatch between the steady pressures a more systematic approach is taken here by using the measured steady pressures themselves to derive equivalent profiles by means of an inverse subsonic method due to Weber (1) for calculating steady pressures. The same profile is then also used to calculate the unsteady pressures for the motion phase that follows the steady calculation phase.

If the operators for the transonic and inverse procedures are denoted by T and W respectively, then the equivalent profile $z(x)$ should satisfy

$$Cp_{exp} = Tz \qquad (1)$$

A first approximation to the desired profile z is

$$z_1 = WCp_{exp} \qquad (1a)$$

so that, from Eq. 1,

$$z_1 = WTz$$

Since the T and W operators are approximately equivalent, we can set

$$WT = I + \varepsilon$$

so that

$$z_1 = WTz = (I + \varepsilon)z$$

$$= z + z\varepsilon \qquad (2)$$

is a first approximation to z. The resulting pressure is

$$Cp_1 = Tz_1$$

An estimate for εz can be obtained by calculating a new profile z_2

$$z_2 = WCp_1 = WTz_1$$

$$= (I + \varepsilon)z_1$$

$$= z_1 + \varepsilon(I + \varepsilon)z$$

so that

$$\varepsilon z = z_2 - z_1 - \varepsilon\varepsilon z \qquad (3)$$

$$= -r(z_2 - z_1)$$

where the unknown term $\varepsilon\varepsilon z$ is taken care of by the empirical factor r. Substituting

εz into Eq.2, we get

$$z = z_1 + r(z_2 - z_1) \qquad (4)$$

for the desired profile. The factor r was set at -0.6, and seems to work for a wide range of profiles (5). The calculation of z(x) thus involves two inverse and one TSP calculation.
One of the equivalent section profiles of the wing under consideration, derived by this method is shown in Fig. 2, together with the original geometrical profile for comparison, in the form of local profile slope versus x/c. There is a rough agreement over most of the chord, with the equivalent profile having a slightly higher slope over the front part, and vice versa. The most significant deviation occurs at the trailing edge on the lower surface, where the equivalent profile shows a noticeable decrease in camber that can be interpreted as the differential thickening of the boundary layer there, tending to lower the circulation and to shift the shock position forward.

III. Derivation of the correction matrix

For linear aerodynamics (small airfoil thicknesses, small amplitude, subsonic flow) the DL method relates pressure and downwash by the relations.

$$Cp = A_3 \alpha \qquad (5)$$

$$Cp = A_2^* \alpha \qquad (6)$$

where the A's are the matrices of the AIC's for three- and two-dimensional flows respectively, and α is the non-dimensional complex downwash. If the points of the DL grid are grouped into strips, the n*n matrix A can be partitioned into submatrices, each submatrix representing the influence of any one strip on any other, with the off-diagonal matrices being non-zero in general.

A second n*n matrix A with the same partitioning scheme may be construed, which has zero off-diagonal submatrices, and its diagonal matrices equal to A_2^*, so that the pressure

$$Cp = A_2 \alpha \qquad (7)$$

corresponds to the pressure distribution given by strip theory, which omits the mutual interaction terms between sections. The wing pressure distribution can now be expressed as

$$Cp_3 = A_3 \alpha = A_3 A_2^{-1} A_2 \alpha . \qquad (8)$$

so that

$$Cp_3 = QCp \qquad (9)$$

with $Cp = A_2 \alpha \qquad (10)$

and $Q = A_3 A_2^{-1} \qquad (11)$

The matrix Q in Eq. 9 can be seen to be a multiplicative correction matrix for strip-theory pressures. An additive correction may also be derived, by the argument

$$Cp_3 = QCp + Cp - Cp$$

$$= Cp + (Q - I)Cp$$

or $$Cp_3 = Cp + SCp \qquad (12)$$

where $S = Q - I = A_3 A_2^{-1} - I \qquad (13)$

Both correction methods will yield results identical to those of Eq. 5, which are correct within the assumptions of the Doublet-Lattice method, as long as strictly subsonic flows are involved.

In this paper the method is extended to transonic flow by replacing the matrix A_2 in Eq. 10 by the transonic operator F, so that

$$Cp = F(\alpha) \qquad (14)$$

The matrix A_2 in the correction matrix S Eq. 13 is, however, left unchanged, the assumption being that the correction matrix S depends mainly on the wing planform, regardless of the flow type, and less on Mach number and reduced frequency.

Furthermore, in the case of a swept wing the behaviour of any shocks on the wing is more likely to depend on the Mach number of the flow normal to an effective sweep line, M cos Λ rather than on the free-stream Mach number M. Therefore all TSP calculations here were made with the normal Mach number based on the sweep of the quarter-chord line. Correspondingly the matrix A_2 was also based on the normal Mach number, and the pressure coefficients were referred to the normal dynamic pressure.

Although the two correction methods are basically equivalent the additive procedure was selected for the calculation of Cp_3. The reasons for this choice were mainly due to numerical considerations. The additive term SCp in Eq. 12 is generally smaller than Cp, and can therefore be calculated on a much coarser DL-grid than Cp. Furthermore the rows of the diagonal matrices of S show a much smoother variation with the streamwise coordinate x than those of Q.

IV. Alternative formulation of the problem

The procedure may also be reformulated as a correction on the downwash rather than the pressures, i.e.

$$Cp_3 = A_2 A^{-1}{}_2 A_3 \alpha$$

or $Cp_3 = A_2 \bar{\alpha}$
with the equivalent downwash given by

$$\bar{\alpha} = R \alpha \qquad (15)$$

and $$R = A_2^{-1} A_3 \qquad (16)$$

By replacing, as before, the matrix A_2 in Eq. 14 by the transonic operator F, Cp_3 can be calculated for transonic flow. However, this method was not used here, since in general $\bar{\alpha}$ exhibits phase lags within a given wing section, and would involve a modification of the TSP program, which was not done. Furthermore, it is somewhat difficult to deduce the motion of an airfoil in the time-domain from its complex downwash, since a term of the form $\exp(i\omega(t-x/U))$ of arbitrary amplitude can be added to the motion without changing the complex downwash.

V. Results and Discussion

The procedures described above were applied to a half-wing wind tunnel model of a transport aircraft with supercritical profiles, with a half-span of 1.1 meters, a full-span aspect ratio of 8.8, and a quarter-chord sweep-angle of 28°. To generate unsteady pressures the entire wing was given a harmonic oscillation in pitch at 40 Hz about a swept axis, corresponding to a reduced frequency of 0.27 at M = 0.78, and 0.25 at M = 0.83 based on mean aerodynamic chord. The wing was braced by cables at the wing tip to eliminated elastic bending.

Figure 1 shows the wing planform, the location of the pitch axis, and the location of the three streamwise sections at which both steady and unsteady pressures were measured. The measurements were made in the ONERA S2 wind tunnel at Modane, France. After putting the measured steady pressures for a subsonic Mach number (0.73) through the two-dimensional Weber-TSP procedure, the resulting equivalent profile was used to calculate the steady pressures at the three sections for two higher Mach numbers, 0.78 and 0.83. Figures 3 and 4 show the calculated pressure distributions for the two Mach numbers and sections 2 and 3, together with the measured pressures, the pressure coefficients being based on the normal dynamic pressure. The agreement between experiment and calculation is seen to be good, especially for the lower Mach number. The shock at the rear of the top surfaces is somewhat overestimated for Mach 0.83. This is probably due to the fact that the inverse Weber procedure does not take account of the shock-boundary layer interaction.

Figure 5 shows the steady pressures on section 1 for Mach 0.78 and 0.83, where the agreement is not as good, the major discrepancies being on the lower surface, where the engine pod (at η = 0.35) is likely to constrict the flow. The agreement for the top surface is as good as for the other two sections.

To determine the unsteady pressure distributions, the TSP-calculations were continued for the equivalent profiles executing a harmonic pitching motion about the local pitching axis. The resulting two-dimensional pressures Cp were then corrected as indicated by Eq. 12 to give the three-dimensional pressure distribution Cp_3.

The results of the calculations are shown in Fig. 6 to 9 as plots of unsteady pressure coefficients divided by the pitch amplitude against x/c(y) together with the appropriate measured pressure coefficients, for the two outtboard sections, and Mach 0.78 and 0.83.

Inspection shows firstly that the correction for three-dimensional effects is very small for this wing and the selected wing sections, and is within the range of experimental scatter. This is primarily due to the high aspect ratio (8.8) of the wing, and the fact that tip effects become noticeable only beyond 90% of the wing span, while the outermost measurement section 3 is located at 88%. However, the corrected pressures lie, in general, closer to the measured ones than the uncorrected ones.

The 3 D corrections probably would have been more pronounced for a wing with a lower aspect ratio; however, measured pressures for such a wing were not available to the author.

Inspection of Fig. 6 to 9 shows further that the calculated and measured pressures in general agree well for the bottom surface of the wing. There are, however, considerable discrepancies in the pressures on the top wing surface. For the lower Mach number (0.78) these are confined to the suction peak near the leading edge, which is overestimated by the calculation, though it is brought down somewhat by the 3D correction. The pressures for the rest of the chord are in reasonable agreement.

The largest discrepancies occur on the top surface for the higher Mach number (0.83). At section 2 (Fig. 8) the peak due to the shock on the rear profile agrees reasonably well in size. The calculated peak, however, lies much further downstream than the measured one. A look at the corresponding steady pressure distribution (Fig. 4, top) shows that the calculated values indicate indeed a more rearward position for the shock, but not as much as evidenced by the unsteady pressures. An explanation for this might be that the maximum value of the shock peak actually lies further downstream, but was not captured by the transducers. This is corroborated by the much smaller discrepancy in the location of the phase jumps across the shock, which are often a more reliable indicator of shock locations.

Much the same can be said about the second peak at about 15% of chord (Fig. 8 and 9, top) due to the small fluctuation in the steady pressures ahead of the shock (Fig. 4). The calculated steady pressures model the measured ones rather well, as far as location is concerned, but the calculated unsteady peaks lie upstream of the measured ones. The leading edge suction peak is, however, reproduced quite well by the calculation.

Part of the explanation for the observed discrepancies, besides a possible failure to capture shock peaks, is that the experimental pitch amplitude was rather small (0.25 deg) because of power limitations, and that the ensuing small unsteady pressures could be rather sensitive to wind tunnel turbulence or small surface irregularities.

Conclusion

A method has been described which makes maximum use of transonic calculation methods for planar flow, subsonic methods for three-dimensional flow, and measured steady pressures to calculate transonic unsteady flow around a wing of moderate to high aspect ratio. Using measured steady pressures to develop equivalent profiles eliminates the need for estimating the steady induced angle of attack along the wing span, and some steady boundary layer effects.

Agreement with measurement is, is general, quite good for the lower Mach number investigated, but only moderate for the higher Mach number of 0.83. This was felt to be due, in some part, to the small pitch amplitude of the wing during measurement.

The 3D corrections for unsteady flow were rather small for the high-aspect-ratio wing and the reduced frequency investigated. To test the applicability of the 3D correction, a wing of a lower aspect ratio should be investigated as a next step.

References

(1) J. Weber: The calculation of the pressure distribution on the surface of thick cambered wings and the design of wings with given pressure distribution.
RAE Reports and Memoranda No. 3026.
June 1953

(2) J.J. Angélini, M. Couston, P. Mulak: Application de l'equation des petites perturbations transsoniques aux calculs d'ecoulements bidimensionnels instationnaires.
ONERA, T.P. No. 1979-140, Sept. 1979

(3) R. Houwink, A.N. Kraan, R.J. Zwaan: A wind- tunnel study of the flutter characteristics of a supercritical wing.
AIAA Paper 81-0651, 1981

(4) A. Steiginga, J.J. Meijer: A revised quasi 3-dimensional concept to determine unsteady airloads on oscillating high-aspect ratio wings in transonic flow.
NLR TR 82062 L. 1982

(5) H. Zimmermann: Unsteady airloads on super-critical wings.
International Symposium on Aeroelasticity at Nuremberg, Germany.
Oct. 1981

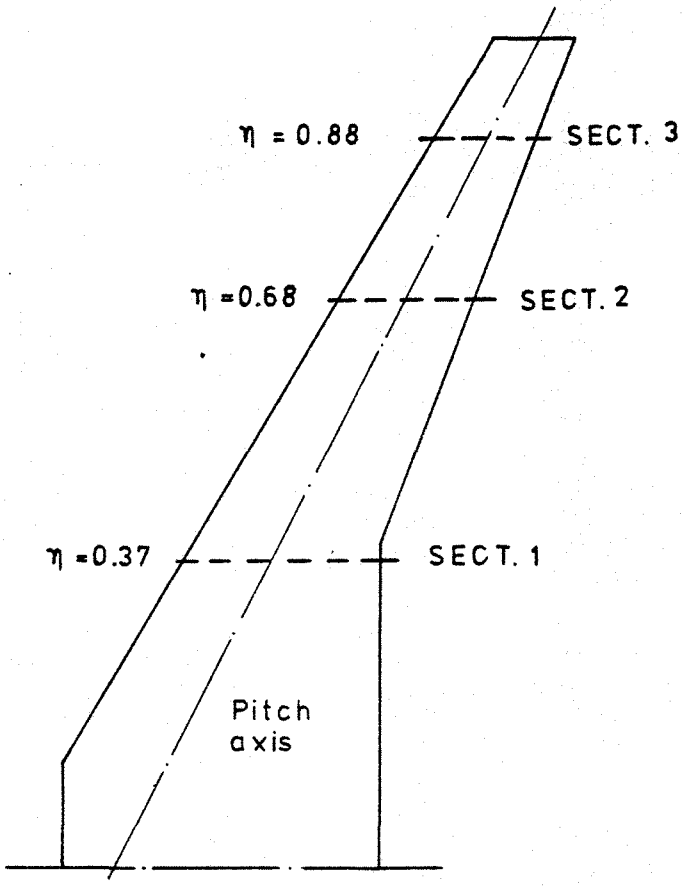

Fig.1 Location of pressure tap sections on model wing
Half - span : 1.1 m

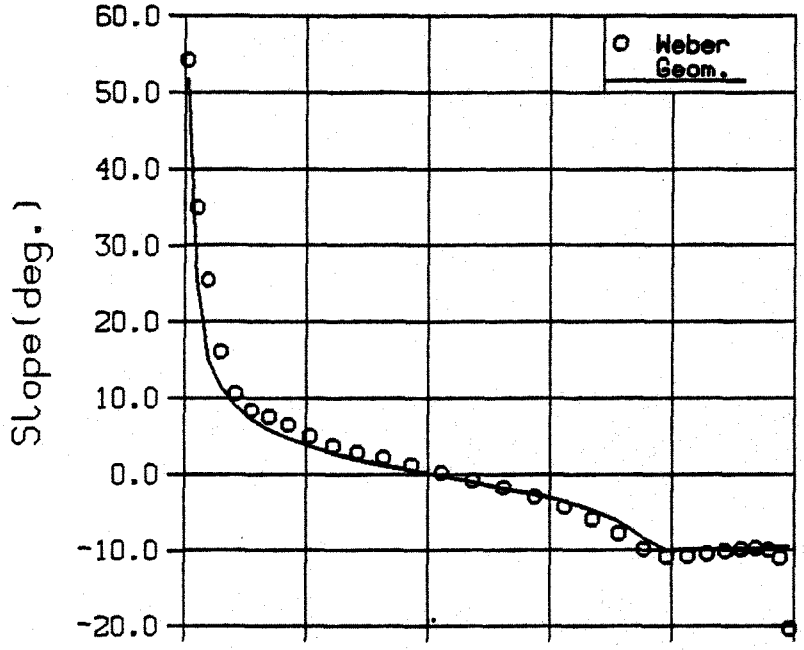

Geometric and Weber profile slopes
for section 2 upper surface

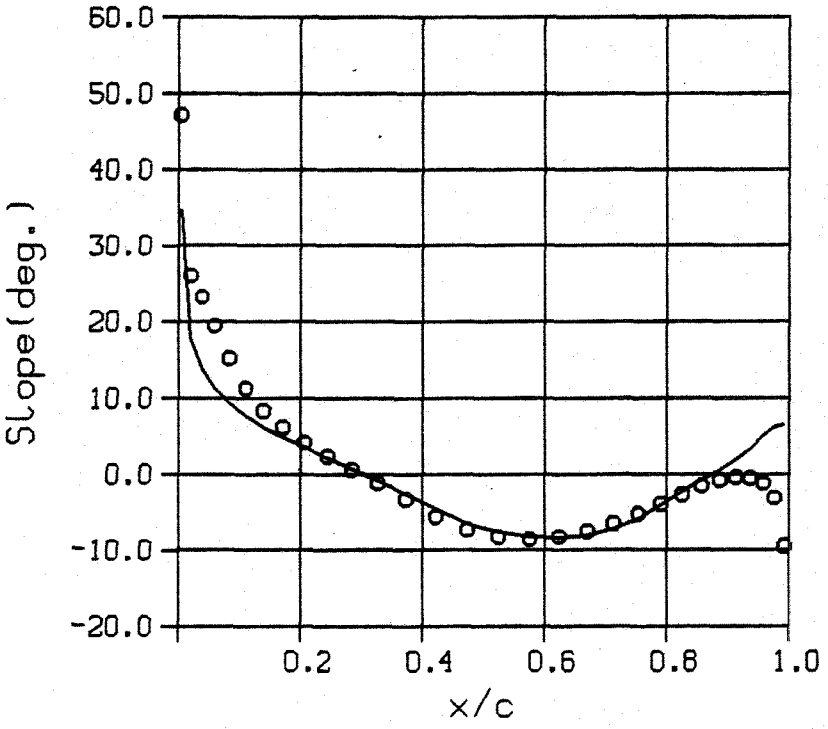

Fig. 2
Geometric and Weber profile slopes
for section 2 lower surface

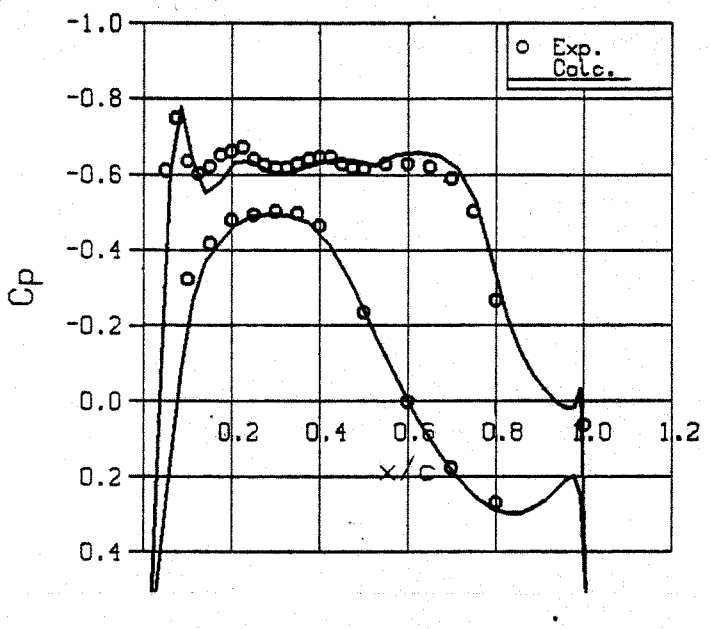

Section 2

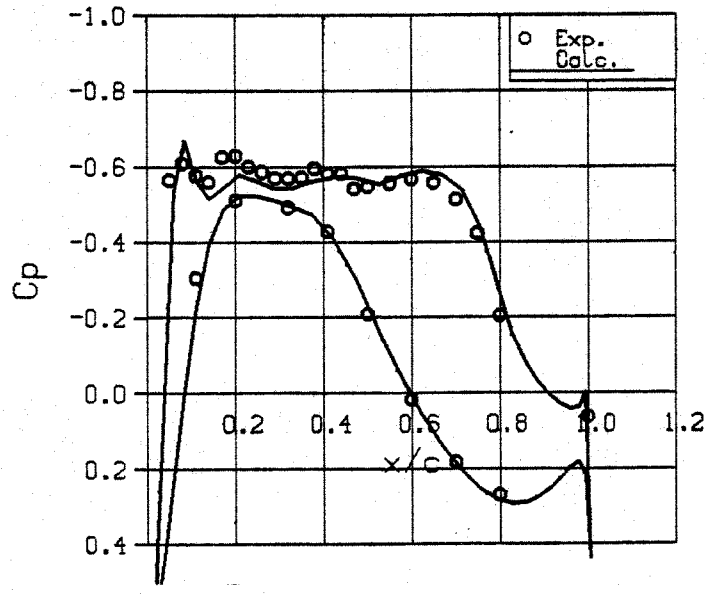

Section 3

Fig. 3 : Steady pressure coefficients for Mach = 0,78, $\alpha = 0°$

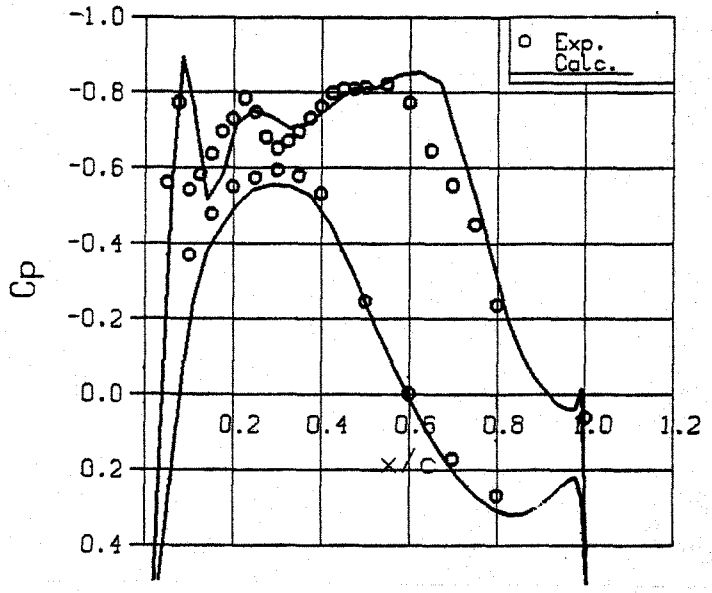

Section 2

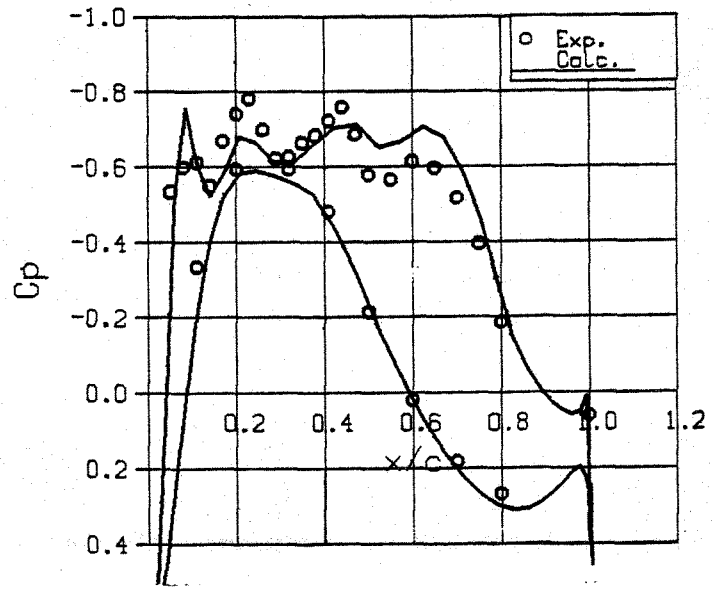

Section 3

Fig. 4: Steady pressure coefficients for Mach = 0,83, $\alpha = 0°$

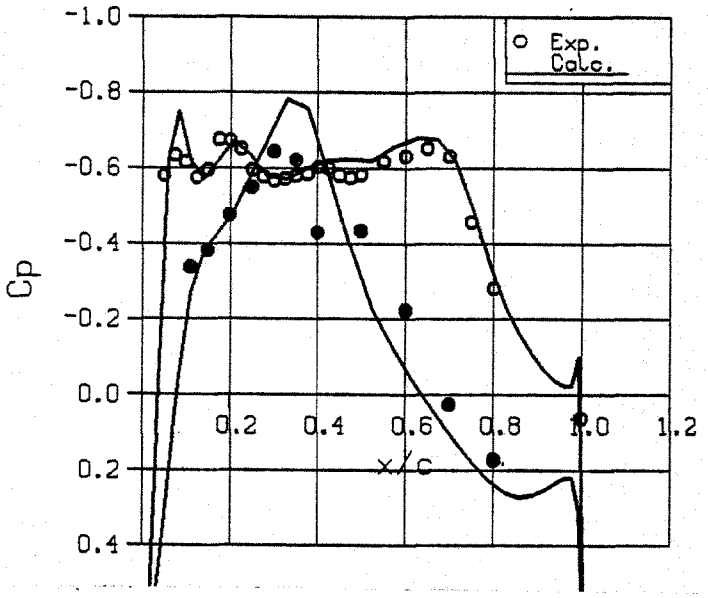

Mach = 0,78

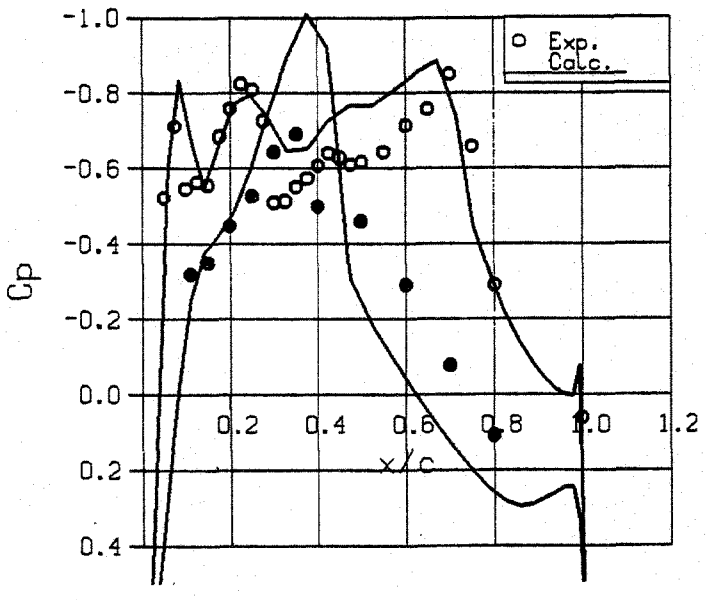

Mach = 0,83

Fig. 5: Steady pressure coefficients for Section 1, $\alpha = 0°$

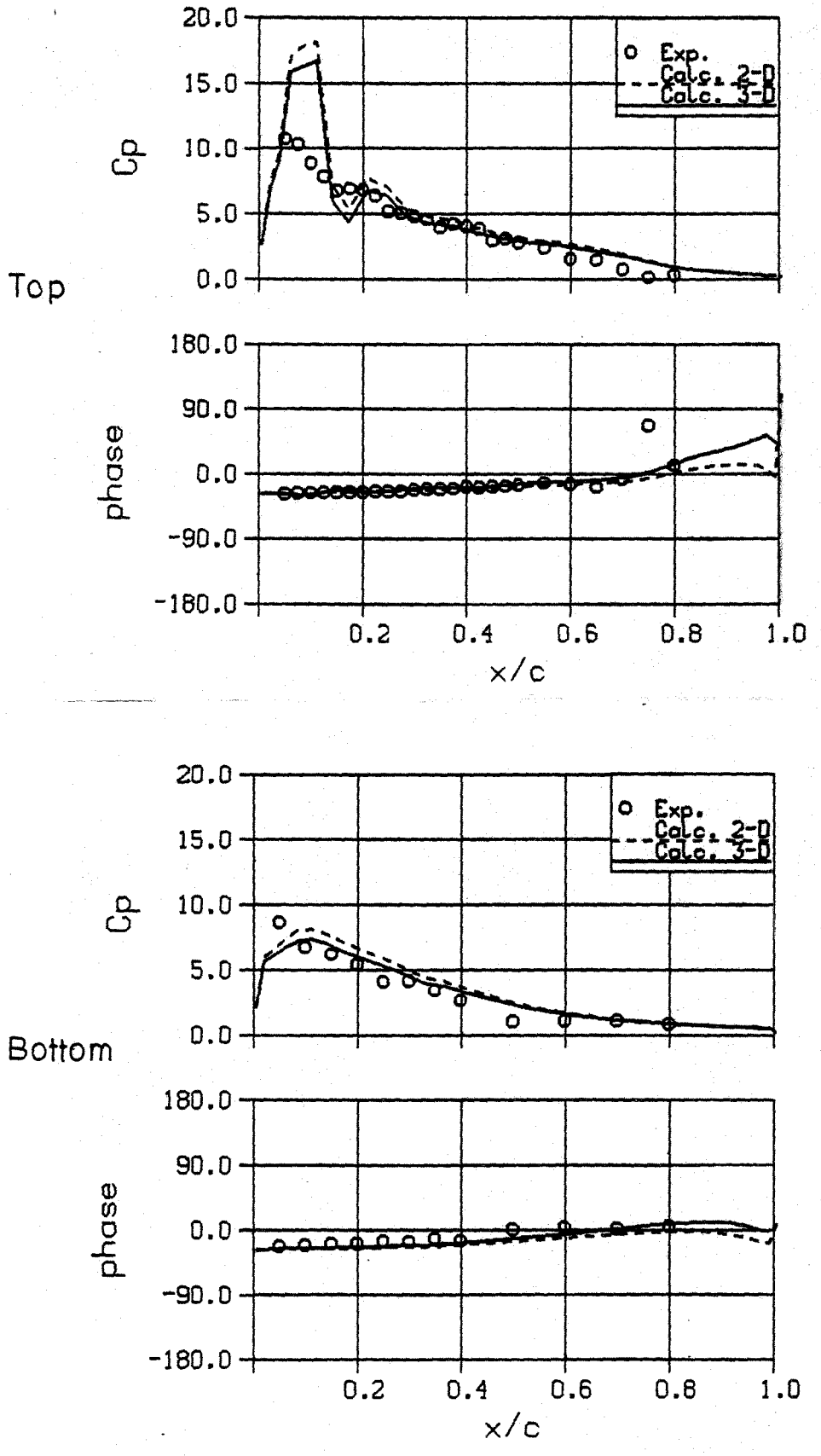

Fig. 6: Unsteady pressure, exp.& calc.
Mach = 0,78, K = 0,27, Sect. 2

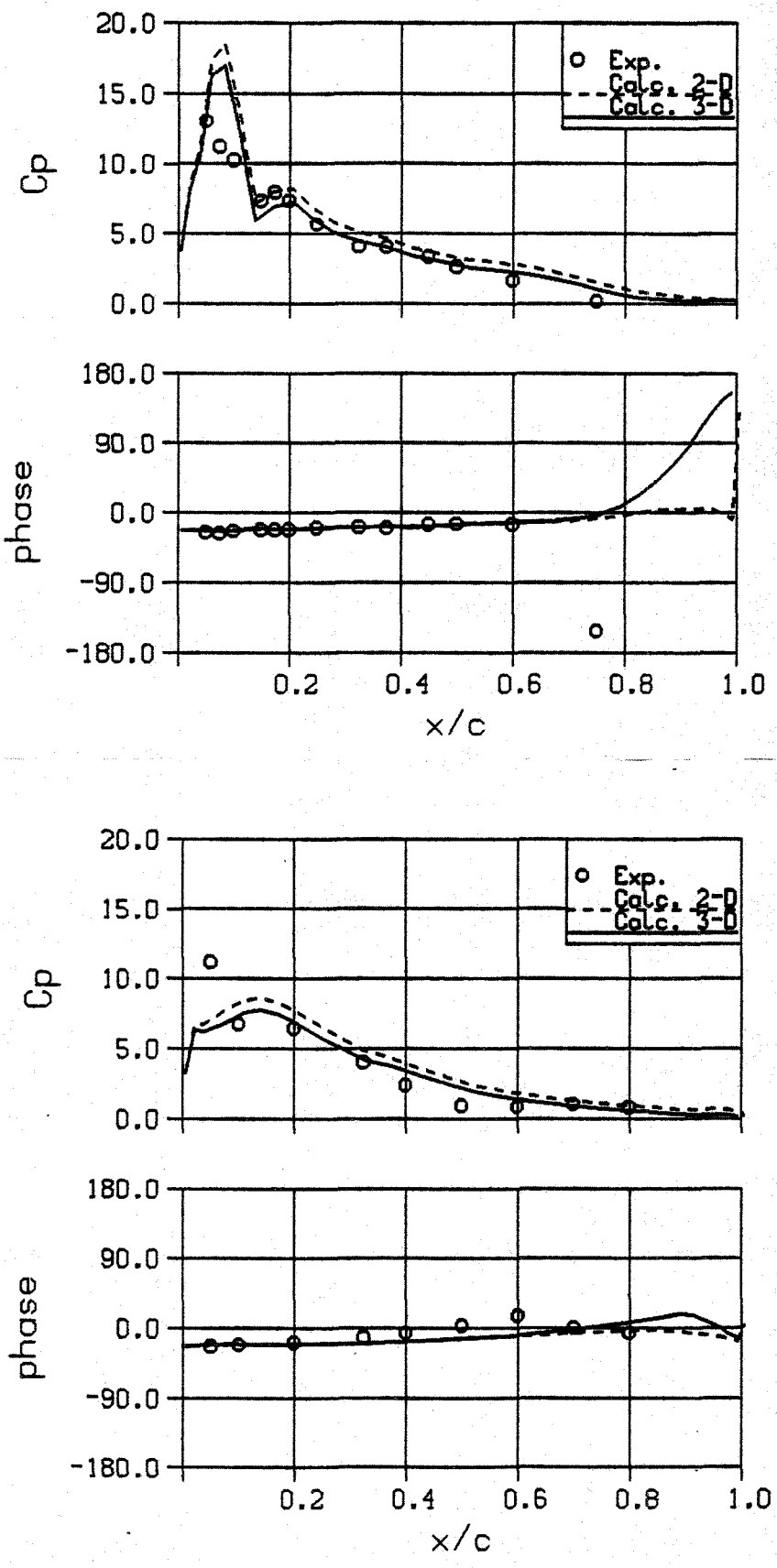

Fig. 7: Unsteady pressure, exp & calc.

Mach = 0,78, K = 0,27 Sect. 3

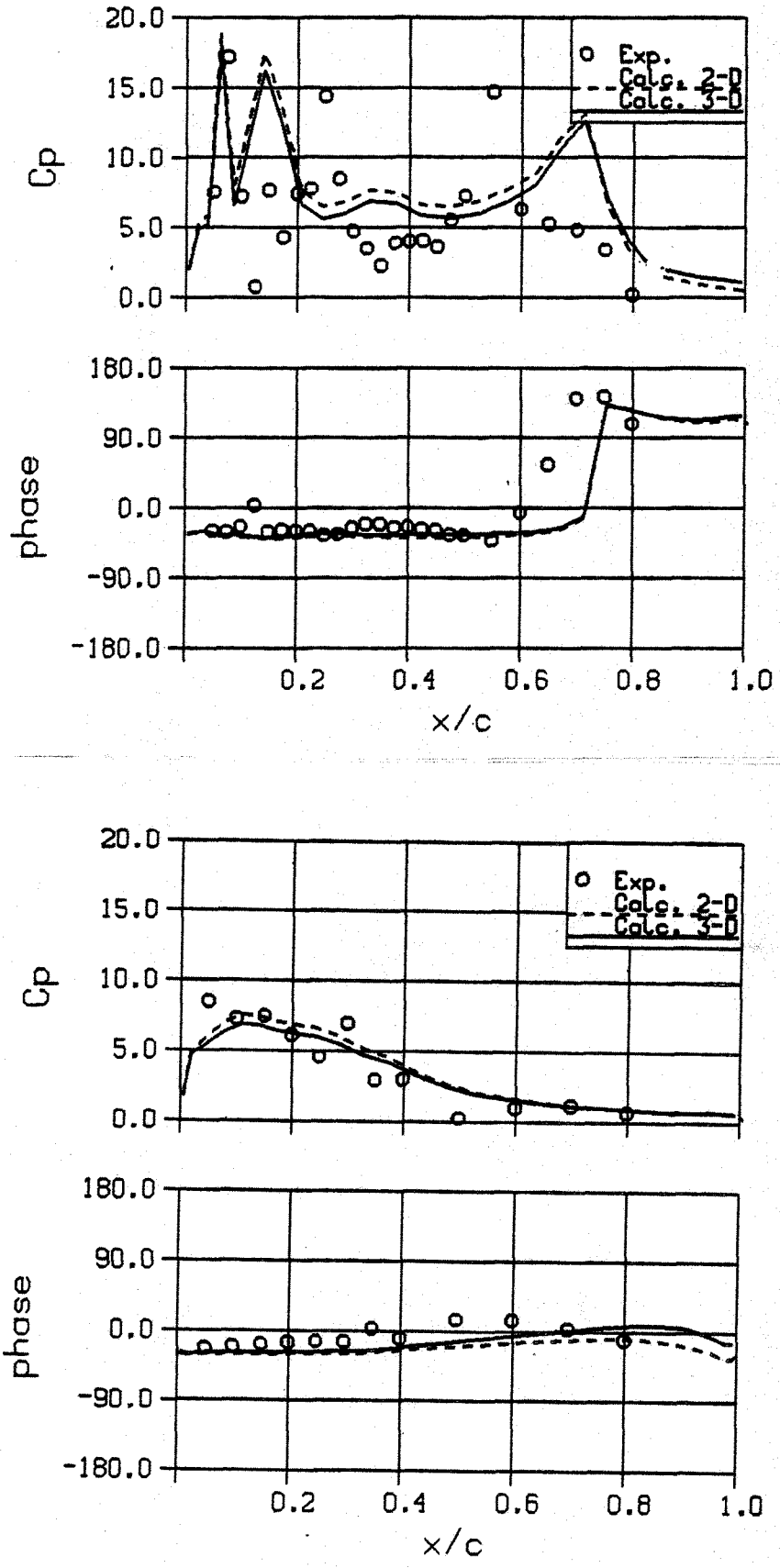

Fig. 8 : Unsteady pressure, exp & calc.
Mach = 0,83, K = 0,25, Sect. 2

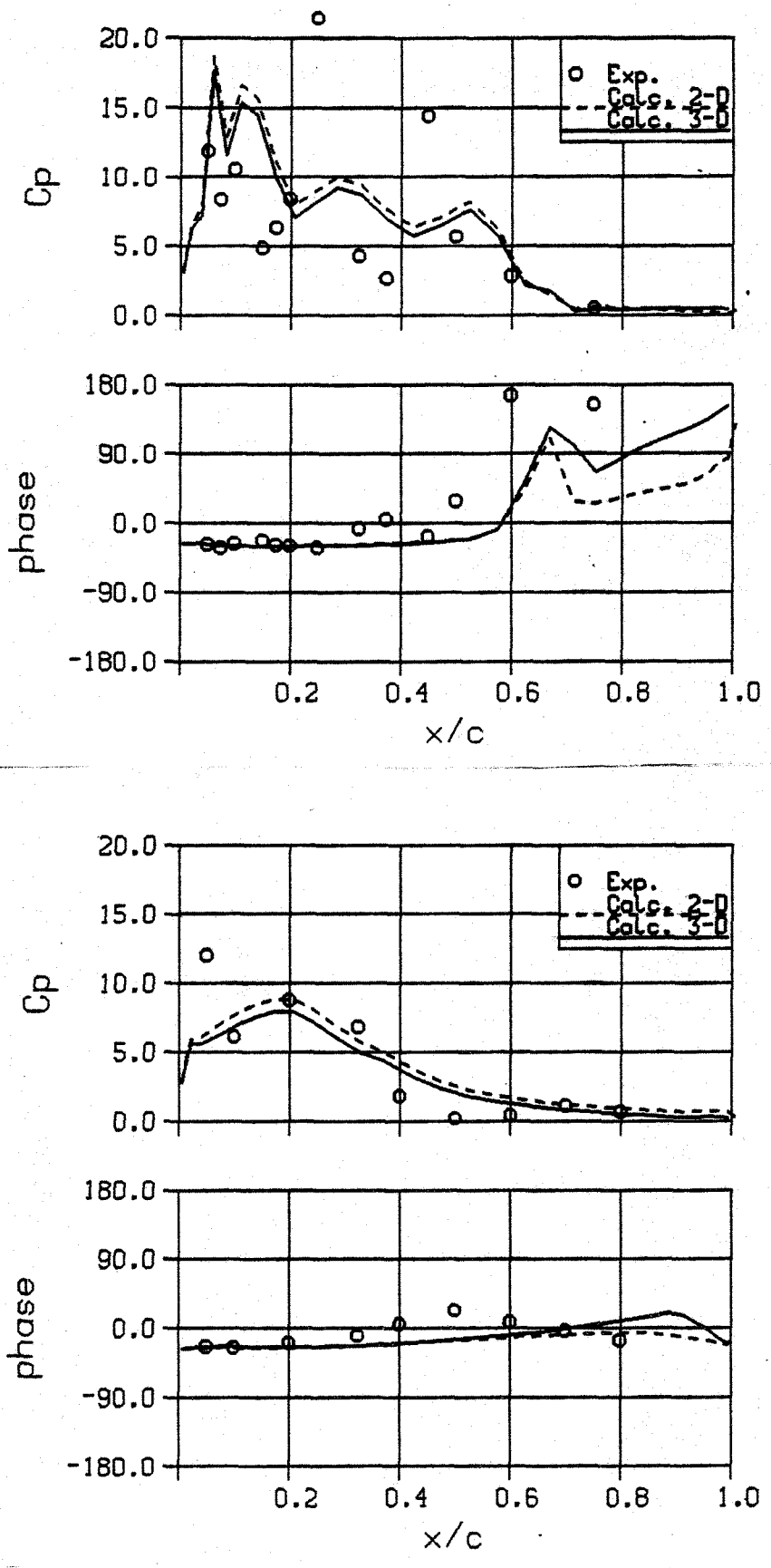

Fig. 9 : Unsteady pressure, exp. \ calc.

Mach = 0,83, K = 0,25, Sect. 3